The Rotational Spectrum and Structure of a Weakly Bound Complex of Ketene and Acetylene

C. W. Gillies,*,† J. Z. Gillies,‡ F. J. Lovas,§ and R. D. Suenram§

Contribution from the Department of Chemistry, Rensselaer Polytechnic Institute, Troy, New York 12180, Department of Chemistry, Siena College, Loudonville, New York 12221, and Molecular Physics Division, National Institute of Standards and Technology, Gaithersburg, Maryland 20899

Received April 5, 1993®

Abstract: Rotational spectra of CH_2CO–C_2H_2, CD_2CO–C_2H_2, CH_2CO–C_2HD, and CH_2CO–C_2D_2 were observed with a pulsed-beam Fabry–Perot cavity Fourier-transform microwave spectrometer. The b-type transitions were split into four states for CH_2CO–C_2H_2 and CD_2CO–C_2H_2, while two states were assigned for CH_2CO–C_2HD and CH_2CO–C_2D_2. All states were fit individually to a quartic Watson Hamiltonian. Relative intensity measurements consistent with nuclear spin statistical weights, deuterium hyperfine effects, and the spectral splitting of isotopic species show that the hydrogen nuclei of ketene and acetylene are exchanged by tunneling motions. The electric dipole moment of CH_2CO–C_2H_2 was measured to be $\mu_a = 0.227(67) \times 10^{-30}$ C m [0.068(20) D] and $\mu_b = 4.707(3) \times 10^{-30}$ C m [1.411 (1) D]. A planar structure is found for the complex (inertial defect, $\Delta = 0.4101$ u Å^2) with a distance of 3.601(1) Å between the center of mass of acetylene and the carbonyl carbon of ketene. The preferred geometry obtained from the moment of inertia data corresponds to the molecular axes of ketene and acetylene tilted by ~25° from parallel alignment with an acetylenic hydrogen directed toward the oxygen of ketene. This structure differs from the crossed configuration expected for a $(2\pi_s + 2\pi_a)$ cycloaddition reaction.

I. Introduction

Pulsed-nozzle Fourier-transform microwave spectroscopy has been extensively used to investigate van der Waals complexes composed of monomer subunits which do not chemically react with each other.[1-3] Recently we reported studies of two complexes made up of monomers which react in the gas phase and solution.[4,5] The two complexes, O_3–C_2H_4[4] and O_3–C_2H_2,[5] were formed in supersonic expansions by sampling reacting mixtures of $O_3 + C_2H_4$ and $O_3 + C_2H_2$ (diluted in argon) with a modified pulsed-beam valve. *Ab initio* calculations and microwave spectral data show that both complexes are weakly bound, having binding energies of 3.1 and 3.5 kJ/mol and center of mass monomer separations of 3.29 and 3.25 Å in O_3–C_2H_4 and O_3–C_2H_2, respectively, and small van der Waals bond stretching force constants of approximately 0.03 mdyn/Å.[4,5] The stabilities and structures of the complexes are determined predominantly by electrostatic interactions with no evidence of charge transfer or overlap interactions.

Since the monomers which make up the two complexes actually participate in bimolecular reactions ($O_3 + C_2H_4$ and $O_3 + C_2H_2$), it is important to determine the relation, if any, of the structures of the complexes to the stereochemical properties of the chemical reactions. The conformations of the O_3–C_2H_4 and O_3–C_2H_2 complexes are found to be similar to those predicted for the transition states of the first steps in the reactions by 1,3-dipolar cycloaddition theory.[4,5] In the case of $O_3 + C_2H_4$, there is a great deal of evidence which indicates that the first step is a concerted cycloaddition between the 1,3-dipole, O_3, and the dipolarophile, C_2H_4.[6,7] In terms of orbital symmetry rules, it is thermally allowed and consists of a $(2\pi_s + 4\pi_s)$ cycloaddition where interaction of the HOMO of ethylene with the LUMO of ozone leads to an envelope conformation of the transition state. *Ab initio* calculations of the $O_3 + C_2H_4$ transition state geometry agree with this HOMO–LUMO description.[8]

The geometry of the O_3–C_2H_4 complex closely resembles the envelope conformation of the transition state determined by the *ab initio* calculations.[4,8] This result suggests that van der Waals interactions responsible for binding in the complex mimic the π interactions as dictated by orbital symmetry rules and substantiated by *ab initio* calculations in the transition state. It is important to note that the separation between ozone and ethylene is approximately 1 Å greater in the complex than in the *ab initio* structure reported for the transition state.[8] Hence, the data strongly suggest that the complex falls along the $O_3 + C_2H_4$ reaction coordinate in a shallow well which precedes the transition state.

Ketene chemistry provides important examples to further explore the relation between the structures of weakly bound complexes and reaction stereochemistry. Alkenes and alkynes react with ketenes to give cyclobutanones and cyclobutenones, respectively.[9-11] Woodward and Hoffmann first discussed the ketene-alkene reaction in terms of a concerted $(2\pi_s + 2\pi_a)$ cycloaddition.[12] The transition state is characterized by crossed, mutually perpendicular molecular planes of ketene and the alkene

† Rensselaer Polytechnic Institute.
‡ Siena College.
§ National Institute of Standards and Technology.
® Abstract published in *Advance ACS Abstracts,* September 15, 1993.

(1) Dyke, T. R. *Top. Curr. Chem.* **1984**, *120*, 86.
(2) Legon, A. C.; Millen, D.J. *Chem. Rev.* **1986**, *86*, 635.
(3) Novick, S. E. Bibliography of Rotational Spectra of Weakly Bound Complexes. In *Structure and Dynamics of Weakly Bound Molecular Complexes;* Weber, A., Ed.; Reidel Publishing Co.: Dordrecht, Holland, 1987.
(4) Gillies, J. Z.; Gillies, C. W.; Suenram, R. D.; Lovas, F. J.; Stahl, W. *J. Am. Chem. Soc.* **1989**, *111*, 3073. Gillies, C. W.; Gillies, J. Z.; Suenram, R. D.; Lovas, F. J.; Kraka, E.; Cremer, D. *J. Am. Chem. Soc.* **1991**, *113*, 2412.
(5) Gillies, J. Z.; Gillies, C. W.; Lovas, F. J.; Matsumura, K.; Suenram, R. D.; Kraka, E.; Cremer, D. *J. Am. Chem. Soc.* **1991**, *113*, 6408.
(6) Bailey, P. S. *Ozonation in Organic Chemistry.* Academic Press: New York, 1978; Vol. 1; 1982; Vol. 2.
(7) Kuczkowski, R. L. *1,3-Dipolar Cycloadditions*; Padwa, A., Ed.; Wiley: New York, 1984; p 197.
(8) McKee, M. L.; Rohlfing, C. M. *J. Am. Chem. Soc.* **1989**, *111*, 2497.
(9) *The Chemistry of Ketenes, Allenes and Related Compounds*; Patai, S., Ed.; Wiley: New York, 1980; Parts 1 and 2.
(10) Ghosez, L.; O'Donnell, M. J. *Pericyclic Reactions*; Marchand, A. P., Lehr, R. E., Eds.; Academic Press: New York, 1977; Vol. 2.
(11) Tidwell, T. T. *Acc. Chem. Res.* **1990**, *23*, 273.
(12) Woodward, R. B.; Hoffmann, R. *The Conservation of Orbital Symmetry*; Verlag Press: New York, 1969.

0002-7863/93/1515-9253$04.00/0

as shown in I. This structure results from reactant approaches

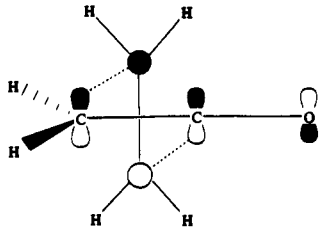

I

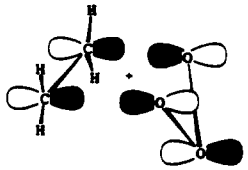

II

which are antarafacial for ketene and suprafacial for the alkene. It differs dramatically from the envelope configuration predicted by a $(4\pi_s + 2\pi_s)$ cycloaddition of ozone to ethylene in II. Recent *ab initio* and semiempirical calculations of the ketene–ethylene reaction show that the orbital interactions are not of the $(2\pi_s + 2\pi_a)$ type as described by Woodward and Hoffman for a cycloaddition process.[13-17] There is only one theoretical study of the ketene–acetylene reaction.[18] The results of the SCF calculations at the STO-3G level are interpreted in terms of a concerted unsynchronous $(2\pi_s + 2\pi_a)$ cycloaddition of ketene to acetylene.[18] The present paper describes an investigation of the ketene–acetylene, CH_2CO–C_2H_2, complex using a modified pulsed-nozzle Fourier-transform microwave spectrometer.[4,5] Analyses of the rotational spectra of four isotopic species have given the geometry of the weakly bound complex. They also reveal internal motions associated with tunneling of the ketene and acetylene hydrogens. These results are related to ketene plus acetylene viewed as a prototypic cycloaddition reaction of alkynes with ketenes.

II. Experimental Section

A pulsed-beam Fourier-transform microwave spectrometer of the Balle–Flygare design[19] was used to observe the rotational transitions of the ketene–acetylene complex. Details of the spectrometer design and operation have been described previously.[20] A dual flow modified pulsed solenoid valve delivered supersonic pulses of the gas mixture to the Fabry–Perot cavity of the spectrometer.[5] Mixtures of 1% ketene in argon and 1% acetylene in argon were flowed through separate 1.6-mm capillary tubing to the high pressure side of the modified valve close to the 0.5-mm orifice. Digital flow controllers continuously regulated the two gas flows through the pulsed valve. The normal gas input of the valve was used to exit the gas mixture and to vent it into an exhaust hood.

Gas flow conditions were adjusted to give optimum molecular signals for acetylene dimer[21] and ketene[22] rotational transitions. The dual flow method permitted either the ketene/argon or acetylene/argon gas flow to be stopped in order to determine whether unknown spectral lines require ketene and/or acetylene. Since a number of unknown complexes were expected to be present in the gas phase, this procedure was needed to establish the possible chemical composition of the complex which produced the unknown spectral lines. The intensities of transitions assigned to the CH_2CO–C_2H_2 complex were optimized at flow rates of 5 cc/min for CH_2CO/Ar and 10 cc/min for C_2H_2/Ar. The most intense transient decay signals were readily seen on a single molecular pulse with a signal to noise ratio of 10 to 1. Line widths for CH_2CO–C_2H_2 were typically 10–15 kHz, and the center frequencies were measured to +4 kHz. For deuterated isotopic species with unresolved deuterium hyperfine structure, the center frequencies were estimated to be a factor of 2–3 less accurate (8–12 kHz).

The procedure used to make the electric dipole measurements with the Fourier-transform spectrometer has been described previously.[23] The $\Delta M_J = 0$ Stark transitions were observed by orienting the dc electric field parallel to the microwave electric field. The $J = 1$–0 $M_J = 0$ transition of OCS and its measured electric dipole moment of $2.3856(10) \times 10^{-30}$ C m [0.715 19(3) D][24] were used to determine the effective static electric field between the Stark plates.

Ketene and its deuterated analogue were prepared by the vacuum pyrolysis of acetic anhydride and deuterated acetic anhydride (99+ atom % D), respectively, and purified by vacuum distillation through a trap maintained at −78 °C.[25] Fully deuterated acetylene was prepared by isotopic exchange between C_2H_2 and a large molar excess of KOD, prepared by dissolving potassium in 99.9% enriched D_2O. The synthesis of partially deuterated acetylene used the same procedure; however, the KOD solution was prepared by mixing H_2O (40% by volume) with D_2O (60% by volume). This acetylene sample contained a mixture of C_2H_2, C_2HD, and C_2D_2 in the ratio of approximately 1:2:1. It was used to observe the microwave spectrum of CH_2CO–C_2HD.

III. Results

A. Microwave Spectra. Uncertainty in the structural configuration of CH_2CO–C_2H_2 and the observation of many lines from other complexes complicated the spectral analysis. A planar geometry as well as a number of conformations which cross the molecular axes of CH_2CO and C_2H_2 will all give rise to an asymmetric top prolate rotor spectrum dominated by b-type R- and Q-branch transitions. A search in the 15–17.5-GHz region revealed the presence of rich spectra which were shown to arise from three van der Waals complexes. Some of these lines required only the CH_2CO/Ar flow, while many transitions disappeared when either the CH_2CO/Ar or C_2H_2/Ar flows were shut off to the molecular pulse valve. A number of lines present in the CH_2CO/Ar flow (no C_2H_2/Ar) were identified and subsequently assigned as transitions arising from the previously unknown Ar–CH_2CO van der Waals complex. These lines disappeared with neon as a carrier gas, as expected for a complex containing argon. However, the transitions which required both ketene and acetylene were also observed in the neon carrier gas flows, and these were ultimately assigned to the CH_2CO–C_2H_2 complex. A large number of unknown lines were observed with either the CH_2CO/Ar or CH_2CO/Ne gas flows (no acetylene flow). These transitions have been tentatively attributed to the weakly bound ketene dimer complex, $(CH_2CO)_2$, and this work is in progress.

The observed microwave transitions of CH_2CO–C_2H_2 are listed in Table I. Only b-type, R- and Q-branch spectra are observed including energy levels to $J = 7$ and $K_p = 2$. Stark effect measurements were used extensively to assign rotational quantum numbers. Quartets are observed for most of the transitions (see Table I), with the larger splitting ranging from ~2 to 6 MHz and the smaller splitting being ~3 MHz or less. Figure 1 illustrates the quartet observed for the 4_{04}–3_{13} transition. The quartets arise from four vibrational (tunneling) states which all have very similar rotational constants. The observed intensities of a number of transitions obtained from free induction decay (FID) in the time domain are consistent with nuclear spin statistical weights expected for internal motions which exchange the pairs of hydrogens in both ketene and acetylene. Consequently, the four components of each rotational transition are assigned to tunneling states of the complex in which the larger splitting arises from the internal motion of acetylene and the smaller splitting from the internal motion of ketene. The tunneling motions of the complex are discussed in more detail in section IIID.

(13) Burke, L. A. *J. Org. Chem.* **1985**, *50*, 3149.
(14) Wang, X.; Houk, K. N. *J. Am. Chem. Soc.* **1990**, *112*, 1754.
(15) Bernardi, F.; Bottoni, A.; Robb, M. A.; Venturini, A. *J. Am. Chem. Soc.* **1990**, *112*, 2106.
(16) Valenti, E.; Pericas, M. A.; Moyano, A. *J. Org. Chem.* **1990**, *55*, 3582.
(17) Yamabe, S.; Minato, T.; Osamura, Y. *J. Chem. Soc., Chem. Commun.* **1993**, 450.
(18) Fang, D.; Fu, X. *Beijing Shifan Daxue Xuebas, Ziran Kexueban* **1991**, *27*, 69.
(19) Balle, T. J.; Flygare, W. H. *Rev. Sci. Instrum.* **1981**, *52*, 33.
(20) Lovas, F. J.; Suenram, R. D. *J. Chem. Phys.* **1987**, *87*, 2010. Suenram, R. D.; Lovas, F. J.; Fraser, G. T.; Gillies, J. Z.; Gillies, C. W.; Onda, M. *J. Mol. Spectrosc.* **1989**, *137*, 127.
(21) Fraser, G. T.; Suenram, R. D.; Lovas, F. J.; Pine, A. S.; Hougen, J. T.; Lafferty, W. J.; Muenter, J. S. *J. Chem. Phys.* **1988**, *89*, 6028.
(22) Johnson, H. R.; Strandberg, M. W. P. *J. Chem. Phys.* **1952**, *20*, 687.
(23) Campbell, E. J.; Read, W. G.; Shea, J. A. *Chem. Phys. Lett.* **1983**, *94*, 69. Coudert, L. H.; Lovas, F. J.; Suenram, R. D.; Hougen, J. T. *J. Chem. Phys.* **1987**, *87*, 6290.
(24) Reinhartz, J. M. L. J.; Dymanus, A. *Chem. Phys. Lett.* **1974**, *24*, 346.
(25) Cox, A. P.; Esbitt, A. S. *J. Chem. Phys.* **1963**, *38*, 1636. Jenkins, A. D. *J. Chem. Soc.* **1952**, 2563.

Table I. Rotational Transitions of CH_2CO–C_2H_2

transition	A_1[a]		A_2		B_1		B_2	
$J'_{K-1,K+1}$–$J''_{K-1,K+1}$	ν_{obsd}[b] (MHz)	$\Delta\nu$[c] (kHz)	ν_{obsd}[b] (MHz)	$\Delta\nu$[c] (kHz)	ν_{obsd}[b] (MHz)	$\Delta\nu$[c] (kHz)	ν_{obsd}[b] (MHz)	$\Delta\nu$[c] (kHz)
3_{12}–3_{03}			7 996.098	−1	7 995.455	2	7 993.648	0
4_{13}–4_{04}			9 295.586	0	9 296.268	−1	9 293.142	−1
1_{11}–0_{00}	10 236.490	−5	10 236.490	3	10 234.087	−6	10 234.056	5
4_{04}–3_{13}	11 701.913	−1	11 701.200	0	11 703.792	−1	11 703.100	2
2_{12}–1_{01}	13 929.337	8	13 929.698	−1	13 926.931	3	13 927.267	−2
7_{25}–7_{16}							15 696.559	0
6_{24}–6_{15}							15 755.309	−1
5_{23}–5_{14}	16 155.040	0	16 155.882	−1	16 149.719	1	16 150.502	1
5_{05}–4_{14}	16 408.009	1	16 407.216	1	16 409.619	0	16 408.842	−2
4_{22}–4_{13}	16 762.936	1	16 763.783	3	16 757.248	−4	16 758.039	1
7_{16}–6_{25}							17 203.671	0
3_{13}–2_{02}	17 371.921	−3	17 372.877	−1	17 369.556	1	17 370.485	−1
3_{21}–3_{12}	17 448.924	3	17 449.460	−2	17 442.977	1	17 443.452	−1
2_{20}–2_{11}	18 085.759	2	18 085.861	0	18 079.625	9	18 079.664	−4

[a] Nuclear spin weight: A_1, 1; A_2, 3; B_1, 3; B_2, 9. [b] The frequency measurements have an estimated uncertainty of 4 kHz. [c] $\Delta\nu$ is the observed minus calculated frequency in kHz from the least-squares fit.

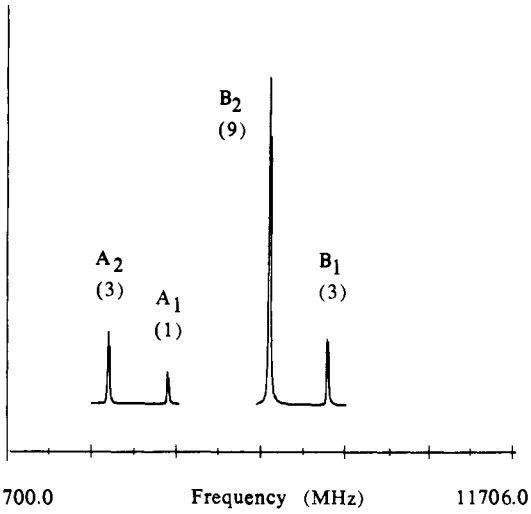

Figure 1. Four tunneling states observed for the $J = 4_{04}$–3_{13} transition of CH_2CO–C_2H_2. Exchange of the acetylenic hydrogens gives rise to the larger A–B splitting, while the smaller A_1–A_2 and B_1–B_2 splittings are due to ketene hydrogen exchange. Nuclear spin statistical weights are given under the symmetry designations of the four states. The frequency markers are at 500 kHz intervals.

For each of the four tunneling states of CH_2CO–C_2H_2, the measured transition frequencies were least-squares fit to the asymmetrical top Watson[26] Hamiltonian in the I^r representation and A-reduced form. Table I lists the residuals from the fits for the transitions of the four states, designated A_1, A_2, B_1, and B_2. Table II gives the rotational constants and five quartic centrifugal distortion constants from the least-squares fits. The fit of the least intense A_1 state included fewer transitions, and δ_J and δ_K were fixed at the A_2 state values of 3.8 and 78 kHz, respectively.

The rotational spectrum of CD_2CO–C_2H_2 was analyzed in the same manner described for CH_2CO–C_2H_2. Many of the b-type transitions were split into quartets as found with CH_2CO–C_2H_2. However, the small splitting assigned to the ketene hydrogen tunneling in CH_2CO–C_2H_2 is reduced to ~0.15 MHz or less in CD_2CO–C_2H_2. Figure 2 illustrates the observed splittings of the 4_{04}–3_{13} transitions of CD_2CO–C_2H_2. The nuclear spin statistical weights are not as certain because the pairs of lines separated by 0.14 MHz in Figure 2 fall within the band width of the microwave cavity, and consequently the intensities are more critically dependent on the cavity resonance positioning relative to the microwave pump frequency. Table III lists the measured transition frequencies and residuals from least-squares fits of the four states. Fits of the less intense A_1 and A_2 states contain fewer $K_p = 2$ lines, and δ_K was fixed at the average of the B_1 and B_2 state values. Table IV gives the spectral constants obtained from the fits for the four states. The higher residuals for CD_2CO–C_2H_2 are due at least in part to the greater uncertainty in locating the line centers of transitions exhibiting partially resolved deuterium hyperfine structure.

The rotational transitions of CH_2CO–C_2HD are split into

(26) Watson, J. K. G. In *Vibrational Spectra and Structure*; Durig, J. R., Ed.; Elsevier: Amsterdam, 1977; Vol. 6, p 1.

Table II. Rotational and Centrifugal Distortion Constants of CH_2CO–C_2H_2[a]

spectral const	A_1	A_2	B_1	B_2
A (MHz)	8389.977(8)	8389.784(2)	8387.505(4)	8387.272(2)
B (MHz)	2372.196(3)	2371.935(4)	2372.154(7)	2371.882(1)
C (MHz)	1846.521(2)	1846.708(3)	1846.507(6)	1846.703(1)
Δ_J (kHz)	15.690(48)	15.665(43)	15.769(76)	15.680(16)
Δ_{JK} (kHz)	50.72(16)	50.13(36)	44.81(63)	44.87(17)
Δ_K (kHz)	9.6(15)	13.50(52)	−59.23(92(	−59.08(47)
δ_J (kHz)	3.8[b]	3.834(26)	3.809(46)	3.7777(89)
δ_K (kHz)	78.0[b]	78.0(16)	79.9(27)	77.48(40)
σ (kHz)[c]	6.0	2.9	5.0	2.8
$\Delta = I_c - I_a - I_b$ (u Å^2)	0.4138	0.3613	0.3943	0.3392

[a] The numbers given in parentheses are one standard deviation of the least-squares fit. [b] Constrained to this value in the fit. [c] Standard deviation of the least-squares fit.

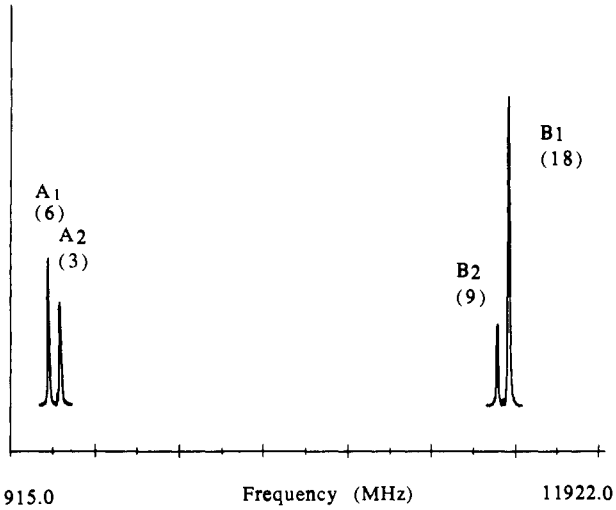

Figure 2. Four tunneling states observed for the $J = 4_{04}$–3_{13} transition of CD_2CO–C_2H_2. The large A–B splitting arises from exchange of the acetylenic hydrogens, while the small A_1–A_2 and B_1–B_2 splittings are due to the ketene deuterium exchange. Nuclear spin statistical weights expected for these tunneling states are listed under the symmetry designations of the states. The frequency markers are at 500-kHz intervals.

Table III. Rotational Transitions of CD_2CO–C_2H_2

transition	A_1[a]		A_2		B_1		B_2	
$J'_{K-1,K+1}$–$J''_{K-1,K+1}$	ν_{obsd}[b] (MHz)	$\Delta\nu$[c] (kHz)	ν_{obsd}[b] (MHz)	$\Delta\nu$[c] (kHz)	ν_{obsd}[b] (MHz)	$\Delta\nu$[c] (kHz)	ν_{obsd}[b] (MHz)	$\Delta\nu$[c] (kHz)
4_{13}–4_{04}					8 710.863	1	8 711.085	3
1_{11}–0_{00}	9 342.317	−15	9 342.317	2	9 335.289	4	9 335.289	−19
4_{04}–3_{13}	11 915.459	−2	11 915.596	2	11 920.931	6	11 920.790	−7
2_{12}–1_{01}	12 890.114	14	12 890.114	15	12 883.079	1	12 883.079	12
4_{22}–4_{13}					14 492.483	−17	14 492.561	6
3_{21}–3_{12}	15 155.437	−9	15 155.519	16	15 137.742	6	15 137.824	−8
2_{20}–2_{11}	15 787.756	9			15 769.518	32	15 769.592	4
3_{13}–2_{02}	16 181.100	−1	16 181.100	−20	16 174.181	−2	16 174.181	−6
5_{05}–4_{14}	16 424.737	0	16 424.890	0	16 429.178	−4	16 429.327	2
2_{21}–2_{12}	17 380.786	−16	17 380.881	−15	17 362.156	−39	17 362.250	29
3_{22}–3_{13}	18 220.289	17	18 220.373	0	18 201.721	−2		
4_{14}–3_{03}	19 267.602	−14	19 267.692	24	19 260.922	−12	19 261.012	26
4_{23}–4_{14}					19 332.209	0	19 332.362	−8
5_{15}–4_{04}	22 228.982	11	22 229.073	−3	22 222.745	35	22 222.816	−17
2_{21}–1_{10}					24 458.210	−13	24 458.175	23

[a] Nuclear spin weight: A_1, 2; A_2, 1; B_1, 6; B_2, 3. [b] The frequency measurements have an estimated uncertainty of 4 kHz. [c] $\Delta\nu$ is the observed minus calculated frequency in kHz from the least-squares fit.

Table IV. Rotational and Centrifugal Distortion Constants of CD_2CO–C_2H_2[a]

spectral const	A_1	A_2	B_1	B_2
A (MHz)	7568.408(14)	7568.368(17)	7561.147(9)	7561.219(13)
B (MHz)	2318.748(7)	2318.769(9)	2318.652(7)	2318.568(12)
C (MHz)	1774.007(4)	1774.010(5)	1773.997(7)	1773.972(10)
Δ_J (kHz)	13.58(16)	13.68(19)	14.73(10)	12.81(16)
Δ_{JK} (kHz)	58.19(99)	57.8(18)	44.67(58)	44.64(90)
Δ_K (kHz)	56.2(33)	40.8(47)	−139.2(14)	−118.4(22)
δ_J (kHz)	3.28(13)	3.43(16)	3.80(9)	3.02(15)
δ_K (kHz)	65.5[b]	65.5[b]	67.2(30)	63.8(47)
σ (kHz)[c]	4.3	4.9	8.6	13.4
$\Delta = I_c - I_a - I_b$ (u Å^2)	0.1524	0.1529	0.0820	0.0770

[a] The numbers given in parentheses are one standard deviation of the least-squares fit. [b] Constrained to this value in the fit, average value of B_1 and B_2 state. [c] Standard deviation of the least-squares fit.

doublets. For each transition the magnitude of the splitting is similar to the A_1–A_2 (B_1–B_2) state splitting observed for CH_2CO–C_2H_2 (see Tables I and V) which arises from the ketene hydrogen tunneling motion. The intensity ratio of transitions from the two states designated A_1 and A_2 in Table V could not be determined very accurately due to the small splittings and deuterium hyperfine structure. However, the A_2 state was approximately a factor of 2–3 more intense than the A_1 state, which is consistent with the 3:1 nuclear spin statistical weights expected for a ketene hydrogen tunneling motion. In section IIIC it will be shown that the complex has a planar geometry (see Figure 3). Two C_2HD isomers are possible, but only the one with the deuterium bonded to the oxygen of ketene is observed presumably because the second isotopic form is of higher energy and is not populated in the cold pulsed beam.

The deuterium hyperfine structure was resolved for a number of the CH_2CO–C_2HD A_1 and A_2 state transitions. Table V summarizes the observed line frequencies of the two states and also includes the hypothetical deuterium quadrupole unsplit frequencies obtained from the hyperfine structure analysis. The unsplit line centers and quadrupole coupling constants were determined by an iterative fit of the measured hyperfine components listed in Table V using a first-order nuclear electric quadrupole interaction.[27] The overall standard deviations of the hyperfine fits for the A_1 and A_2 states are 1.6 and 1.7 kHz, respectively. The A_1 and A_2 unsplit line frequencies listed in Table V were least-squares fit to the Watson Hamiltonian for an asymmetric top in the I^r representation and A-reduced form.[26] Table VI lists the spectroscopic constants from these fits. The fit of the less intense A_1 state did not contain sufficient lines to determine δ_K. Consequently, δ_K was fixed at the A_2 state value of 71 kHz.

As with CH_2CO–C_2H_2 and CD_2CO–C_2H_2, four vibrational states are expected for the CH_2CO–C_2D_2 isotopic species due to tunneling of the ketene hydrogen and acetylene deuterium atoms. However, unlike CD_2CO–C_2H_2, the deuterium hyperfine structure is resolved for a number of the CH_2CO–C_2D_2 rotational transitions. In addition, hyperfine components of the four states are not separated from one another because the ketene hydrogen and acetylene deuterium tunneling splittings are small and not very different. These complicating factors have permitted the spectral assignments of only the two most intense tunneling states.

An investigation of the nitrogen–water complex[28] provided guidance in the spectral analysis of CH_2CO–C_2D_2. The acetylene tunneling motion makes the deuterium nuclei equivalent, and consequently, one set of deuterium quadrupole coupling constants determines the hyperfine components of a rotational transition. Each deuterium nucleus has a nuclear spin of 1. The two equivalent spins couple to each other to give $I_1 + I_2 = I_D$ where $I_D = 0$, 1, and 2. Coupling of I_D to the overall rotation of CH_2CO–C_2D_2 yields $F = I_D + J$. The $I_D = 0$ and 2 nuclear spin functions are symmetric with respect to deuterium exchange, while the $I_D = 1$ spin function is antisymmetric. Symmetry designations of the four vibrational states which arise from the ketene and acetylene tunneling motions are described in section IIID. These are A_1, A_2, B_1, and B_2, where the acetylene motion gives rise to the A–B splitting. The nuclear spin statistical weights are 6:18:3:9, respectively, for A_1:A_2:B_1:B_2. Since the deuterium nuclei act as bosons upon exchange by tunneling, the $I_D = 0$ and 2 spin functions must combine with the symmetric A states and the $I_D = 1$ spin function with the antisymmetric B states. This means the two most intense tunneling states, A_2 and B_2, will contain either the $I_D = 0$ and 2 or $I_D = 1$ components, respectively, for a given rotational transition.

(27) Gordy, W.; Cook, R. L. In *Technique of Organic Chemistry*; Weissberger, A., Ed.; Interscience: New York, 1970; Vol. IX.

(28) Leung, H. O.; Marshall, M. D.; Suenram, R. D.; Lovas, F. J. *J. Chem. Phys.* **1989**, *90*, 700.

Table V. Rotational Transitions of CH_2CO–C_2HD

transition		A_1[a]				A_2			
$J'_{K-1,K+1}$–$J''_{K-1,K+1}$	F′–F″	ν_{obsd}[b] (MHz)	$\Delta\nu_{hfs}$[c] (kHz)	ν_0[d] (MHz)	$\Delta\nu_0$[e] (kHz)	ν_{obsd}[b] (MHz)	$\Delta\nu_{hfs}$[c] (kHz)	ν_0[d] (MHz)	$\Delta\nu_0$[e] (kHz)
3_{12}–3_{03}				7 752.961[f]	−3			7 751.098	1
	3–3					7 751.068	11		
	4–4					7 751.105	−7		
	2–2					7 751.127	−3		
4_{13}–4_{04}				9 078.990[f]	0			9 075.887	−1
	4–4					9 075.855	14		
	5–5					9 075.892	−12		
	3–3					9 075.917	−3		
1_{11}–0_{00}				9 910.749[f]	11			9 910.557	−3
	2–1					9 910.550	2		
	1–1					9 910.596	−6		
4_{04}–3_{13}				11 740.056	1			11 739.748	1
	4–3	11 740.024	−3			11 739.717	−3		
	5–4	11 740.067	2			11 739.760	3		
2_{12}–1_{01}				13 544.364	−12			13 544.590	0
	1–0					13 544.525	−5		
	3–2	13 544.361	9			13 544.582	4		
	2–1	13 544.400	−10			13 544.636	1		
3_{21}–3_{12}								16 639.111[f]	1
3_{13}–2_{02}				16 926.198	9			16 927.000	8
	2–1	16 926.167	3			16 926.971	4		
	4–3	16 926.179	6			16 926.985	−3		
	3–2					16 927.039	0		
2_{20}–2_{11}				17 273.670	0			17 273.190	−1
	1–1	17 273.614	5			17 273.134	1		
	3–3	17 273.661	6			17 273.177	3		
	2–2	17 273.720	−2			17 273.243	−4		
2_{21}–2_{12}				18 829.513[f]	−3			18 827.807[f]	6
3_{22}–3_{13}				19 644.982	4			19 642.594	0
	3–3	19 644.948	2			19 642.559	−8		
	4–4	19 644.991	−3			19 642.610	7		
4_{14}–3_{03}				20 101.677	−6			20 103.198	−2
	5–4	20 101.660	−4			20 103.179	−7		
	4–3	20 101.717	3			20 103.238	6		
4_{23}–4_{14}								20 738.989	0
	4–4					20 738.952	−5		
	5–5					20 739.004	3		
5_{15}–4_{04}				23 140.855	1			23 143.107	−1
	6–5	23 140.833	−10			23 143.087	−9		
	5–4	23 140.895	9			23 143.145	10		
2_{21}–1_{10}								26 096.295	−7
	3–2					26 096.285	0		
	2–2					26 096.302	−2		
	2–1					26 096.355	15		

[a] Nuclear spin weight: A_1, 1; A_2, 3. [b] The measurement uncertainty is estimated to be 4 kHz. [c] $\Delta\nu_{hfs}$ is the observed minus calculated frequency in kHz from the least-squares fit to the quadrupole coupling constants. [d] ν_0 are the unsplit center frequencies obtained from the quadrupole fit. [e] $\Delta\nu_0$ are the observed minus calculated frequencies from the least-squares fit of ν_0 to the rotational and centrifugal distortion constants. [f] N_o hyperfine components are observed; transition used only for the unsplit line fit.

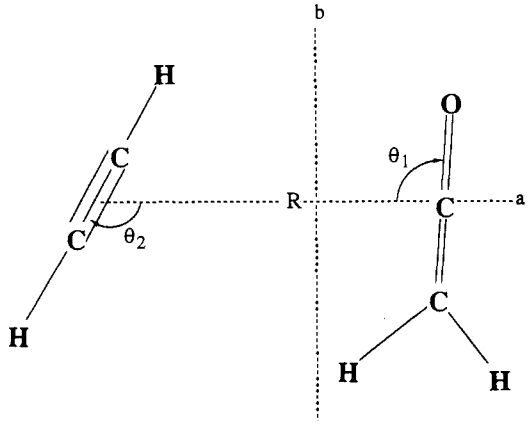

Figure 3. Structural parameters R, θ_1, and θ_2 determined from the microwave data for a planar CH_2CO–C_2H_2 complex. R is the distance between the center of mass of acetylene and the carbonyl carbon of ketene. θ_1 and θ_2 define the orientation of ketene and acetylene, respectively, to R.

A first-order treatment of the nuclear electric quadrupole interaction of the two deuterium nuclei (assumed to be equivalent due to tunneling in the complex) was used to iteratively fit the assigned hyperfine components of the A_2 and B_2 states listed in Table VII. This fit gave the set of quadrupole coupling constants

Table VI. Spectral Constants of CH_2CO–C_2HD and CH_2CO–C_2D_2[a]

spectral const	CH_2CO–C_2HD		CH_2CO–C_2D_2	
	A_1	A_2	A_2	B_2
A (MHz)	8093.800(9)	8093.430(4)	7830.338(6)	7829.988(7)
B (MHz)	2347.569(5)	2347.331(4)	2258.601(5)	2258.583(6)
C (MHz)	1816.914(2)	1817.107(5)	1750.697(2)	1750.696(3)
Δ_J (kHz)	14.82(12)	14.60(6)	14.83(11)	14.68(15)
Δ_{JK} (kHz)	44.82(59)	44.72(21)	27.6(4)	25.46(50)
Δ_K (kHz)	−15.1(14)	−13.18(75)	21.0(11)	9.7(14)
δ_J (kHz)	3.75(7)	3.66(3)	3.81(5)	3.73(7)
δ_K (kHz)	71[b]	71.4(22)	71[b]	71[b]
σ (kHz)[c]	1.6	5.2	7	7
$\Delta = I_c - I_a - I_b$ (u Å^2)	0.4346	0.3803	0.3747	0.3703
eQq_{aa} (kHz)	−35.9(120)	−60.7(91)	−44(3)	
eQq_{bb} (kHz)	184.9(98)	179.0(70)	133.7(21)	
eQq_{cc} (kHz)	−149(16)	−118.3(96)	−89.7(27)	

[a] The numbers in parentheses are one standard deviation of the least-squares fit. [b] Constrained to this value in the fit. [c] Standard deviation of the least-squares fit.

Table VII. Hyperfine Rotational Transitions and Deuterium Quadrupole Fit of CH_2CO–C_2D_2

transition				A_2 (I = 0 and 2)[a]	B_2 (I = 1)	
$J'_{K_{-1},K_{+1}}$–$J''_{K_{-1},K_{+1}}$	I	F'	F''	ν_{obsd}[b] (MHz)	ν_{obsd}[b] (MHz)	$\Delta\nu_{hfs}$[c] (kHz)
3_{12}–3_{03}	1	4	4		7 490.395	3
	1	3	3		7 490.430	−3
	2	4	4	7 490.716		1
	2	5	5	7 490.764		−1
4_{13}–4_{04}	1	3	3		8 756.663	−4
	1	5	5		8 756.683	4
	1	4	4		8 756.726	0
	0	4	4	8 756.966		0
	2	5	5	8 757.002		0
	2	6	6	8 757.056		−3
	2	4	4	8 757.073		2
1_{11}–0_{00}	1	1	1		9 580.686	0
	1	2	1		9 580.725	−1
	1	0	1		9 580.787	1
	2	1	2	9 580.974		0
	2	1	0	9 580.974		0
	2	3	2	9 581.047		−1
	0	1	0	9 581.105		2
	2	2	2	9 581.105		−3
2_{12}–1_{01}	1	3	2		13 082.020	0
	2	4	3	13 082.321		1
	2	3	2	13 082.378		−1
2_{20}–2_{11}	1	2	2		16 747.209	2
	1	3	3		16 747.259	−2
	2	2	2	16 747.984		0
	2	3	3	16 748.088		0

[a] Nuclear spin weight: A_2, 18; B_2, 9. [b] The frequency measurements have an estimated uncertainty of 4 kHz. [c] $\Delta\nu_{hfs}$ are the observed minus calculated frequencies from the quadrupole fit.

Table VIII. Rotational Transitions of CH_2CO–C_2D_2

transition	A_2		B_2	
$J'_{K_{-1},K_{+1}}$–$J''_{K_{-1},K_{+1}}$	ν_0[a] (MHz)	$\Delta\nu_0$[b] (kHz)	ν_0[a] (MHz)	$\Delta\nu_0$[b] (kHz)
3_{12}–3_{03}	7 490.745	−4	7 490.403	−1
4_{13}–4_{04}	8 757.033	1	8 756.692	0
1_{11}–0_{00}	9 581.062	5	9 580.719	−2
4_{04}–3_{13}	11 263.607	1	11 263.829	0
2_{12}–1_{01}	13 082.337	6	13 082.011	7
3_{21}–3_{12}	16 139.180[c]	4	16 138.438[c]	0
3_{13}–2_{02}	16 342.428[c]	−2	16 342.118[c]	−7
2_{20}–2_{11}	16 748.040	−2	16 747.249	0
2_{21}–2_{12}	18 237.548[c]	−2		
4_{14}–3_{03}	19 404.352[c]	−8	19 404.090[c]	2
5_{15}–4_{04}	22 334.365[c]	4		

[a] ν_0 are the unsplit center frequencies obtained from the quadrupole fit listed in Table VII. [b] $\Delta\nu_0$ are the observed minus calculated frequencies from the least-squares fit of ν_0 to the rotational and centrifugal distortion constants. [c] No hyperfine components are observed; transition frequency used only for the unsplit line fit.

in Table VI and the unsplit line centers of the A_2 and B_2 state rotational transitions in Table VIII with an overall standard deviation of 6 kHz. The unsplit centers and a few transitions with unresolved hyperfine components were fit separately for the A_2 and B_2 states to the Watson Hamiltonian employed for the other ketene–acetylene isotopic species. Table VI lists the rotational constants and quartic centrifugal distortion constants obtained from these two fits. For the A_2 and B_2 state fits, the distortion constant, δ_K, could not be determined from the measured transitions and, consequently, was fixed at the value found for the intense A_2 state of CH_2CO–C_2HD (Table VI).

Attempts to observe hyperfine components of sufficient rotational lines for spectral analysis of the A_1 and B_1 states were not successful due to lack of intensity as expected for these states which have smaller nuclear spin weights. However, a few of the most intense low J rotational transitions exhibited one or two lines which do not belong to the hyperfine components of the assigned A_2 and B_2 states. It is likely that these lines are the most intense hyperfine components of the A_1 and B_1 states.

B. Dipole Moment Analysis. The electric dipole moment of CH_2CO–C_2H_2 was determined from 20 Stark effect measurements of $\Delta M_J = 0$ components of the 1_{11}–0_{00}, 2_{12}–1_{01}, and 3_{13}–2_{02} transitions. Frequency shifts of these transitions were quadratic functions of the static applied electric field. A least-squares fit of the data to second order perturbation theory determined μ_c to be 0 within the uncertainty of the measurements. Consequently, the data were refit to the a and b components which gave μ_a = 0.227(67) × 10^{-30} Cm [0.068(20) D] and μ_b = 4.707(3) × 10^{-30} Cm [1.411(1) D] with a standard deviation of 4 kHz for the overall fit. The absence of a-type transitions is consistent with the small magnitude of the μ_a dipole component. A total electric dipole moment of 4.713(3) × 10^{-30} Cm [1.413(1) D] for the complex is calculated from the fitted values of μ_a and μ_b. Since the magnitude of the b dipole moment component of the complex is close to the known electric dipole moment of ketene monomer (μ = 4.743 × 10^{-30} Cm (1.422 D) for CH_2CO)[29] and the a dipole component of the complex is almost zero, the C_2 axis of ketene must be aligned nearly parallel to the b inertial axis of CH_2-CO–C_2H_2.

C. Structural Analysis. The inertial defect, $\Delta = I_c - I_b - I_a$, is 0.4101 u Å^2 for the A_1 state of CH_2CO–C_2H_2, which indicates that the complex has a planar equilibrium geometry. Supporting evidence for planarity comes from the small variation in the inertial defects of the A_1 state of CH_2CO–C_2HD (Δ = 0.4346 uÅ^2) and the A_2 state of CH_2CO–C_2D_2 (Δ = 0.3747 uÅ^2) as compared to the inertial defect of CH_2CO–C_2H_2. The change in the inertial defect of the A_1 state of CD_2CO–C_2H_2 (Δ = 0.1524 uÅ^2) relative to CH_2CO–C_2H_2 is larger than the deuterated acetylene isotopic species. This result may indicate that the ketene hydrogens are located slightly out of the complex plane. However, rotations of more than about 10° of the ketene hydrogens about the C=C=O axis of ketene are not compatible with the moment of inertia data. Consequently, a planar geometry is used in the structural analysis of CH_2CO–C_2H_2. The electric dipole measurements and observed inertial defects point to the planar geometry shown in Figure 3, where the b inertial axis of the complex is aligned nearly parallel to the C_2 axis of ketene monomer. This structure is qualitatively similar to the planar bridged geometry of formaldehyde–acetylene complex.[30]

Three structural parameters are required to determine the geometry of a planar complex if the monomer structures of ketene and acetylene are fixed at the r_0 values listed in Table IX. These parameters are identified in Figure 3 and include R, the distance between the carbonyl carbon of ketene and the center of mass of acetylene, and the two angles, θ_1 and θ_2, which define the orientations of ketene and acetylene in the plane of the complex. Twelve moments of inertia obtained from the rotational constants of the four isotopic species (CH_2CO–C_2H_2, CD_2CO–C_2H_2, CH_2-CO–C_2D_2, and CH_2CO–C_2HD) can be used in a least-squares fit to determine R, θ_1, and θ_2. However, a problem arises in the analysis because two structural isomers of CH_2CO–C_2HD are possible, but only one was observed in the cold molecular beam. These two forms of CH_2CO–C_2HD differ by location of the acetylenic deuterium either adjacent to the oxygen of ketene (designated isomer A) or adjacent to the nearest hydrogen of ketene (designated isomer B). Unfortunately, the moment of inertia data for the remaining three isotopic species (CH_2CO–C_2H_2, CD_2CO–C_2H_2, and CH_2CO–C_2D_2) do not contain sufficient structural information to uniquely assign the observed CH_2CO–C_2HD isotopic species to one of the two isomers (A or B). Consequently, two fits of the 12 moments of inertia were carried out to determine R, θ_1, and θ_2. In fit A, the experimental moments of inertia of CH_2CO–C_2HD were assigned to isomer

(29) Fabricant, B.; Krieger, D.; Muenter, J. S. *J. Chem. Phys.* **1977**, *67*, 1576.

(30) Howard, N. W.; Legon, A. C. *J. Chem. Phys.* **1988**, *88*, 6793.

Table IX. Structural Parameters of the CH_2CO–C_2H_2 Complex

Monomer Geometry

	CH_2CO[a]	C_2H_2[b]
r_{CH} (Å)	1.0754	1.0570
r_{CC} (Å)	1.3147	1.2086
r_{CO} (Å)	1.1620	
θ (HCC) (deg)	118.9	
θ (HCH) (deg)	122.2	

CH_2CO–C_2H_2 Geometry

	fit A[c]	fit B[d]
R (Å)	3.601(1)	3.602(1)
θ_1 (deg)	93.1(8)	95.0(7)
θ_2 (deg)	115.7(6)	64.6(4)
σ[e] (u Å^2)	0.20	0.20

[a] Determined from a r_o fit of the I_a and I_b moments of inertia for CH_2CO, CD_2CO, CHDCO, $^{13}CH_2CO$, and $CH_2C^{18}O$: Johns, J. W. C.; Stone, J. M. R. *J. Mol. Spectrosc.* **1972**, *42*, 523. Nemes, L.; Winnewisser, M. *Z. Naturforsch.* **1976**, *31a*, 272. Cox, A. P.; Thomas, L. F.; Sheridan, J. *Spectrochim. Acta* **1959**, *15*, 542. [b] Determined from a r_o fit of the moments of inertia of C_2H_2, C_2HD, and C_2D_2: Fast, H.; Welch, H. L. *J. Mol. Spectrosc.* **1972**, *41*, 203. Palmer, K. F.; Michelson, M. E.; Rao, K. N. *J. Mol. Spectrosc.* **1972**, *44*, 131. [c] Fit of four isotopic species moments of inertia with deuterium in CH_2CO–C_2HD located adjacent to the ketene oxygen (isomer A). [d] Fit of four isotopic species moments of inertia with the deuterium in CH_2CO–C_2HD positioned next to the ketene hydrogen (isomer B). [e] One standard deviation of the overall moment of inertia fit.

A, while in fit B they were assigned to isomer B. Table IX lists the values of R, θ_1, and θ_2 obtained from these fits. Since the overall standard deviations of the fits are virtually identical, the two sets of parameters obtained from fits A and B both satisfy the moment of inertia data equally well. Thus, the moment of inertia data do not distinguish between the two structures.

These structures, designated A and B in Figure 4, differ only by the orientation of acetylene in the complex. Supplementary values of θ_2 (116.0° for A and 64.6° for B) place one acetylenic hydrogen adjacent to the ketene oxygen in A while, the other acetylenic hydrogen is located next to the ketene hydrogen in B. Structure A is preferred over B primarily because the short nonbonded H···H distance of 1.81 Å (see structure B in Figure 4) destabilizes the complex in B. The electrostatic interaction is repulsive since the sum of two hydrogen van der Waals radii is 2.4 Å.

The deuterium electric quadrupole coupling constants, eQq_{aa} and eQq_{bb}, measured for CH_2CO–C_2HD and CH_2CO–C_2D_2 can be used to independently determine the angle, θ_2, by eqs 1 and 2. In these equations, θ_a and θ_b are the projection angles of the

$$eQq_{aa} = eQq(D)[(3\langle\cos^2\theta_a\rangle - 1)/2] \quad (1)$$

$$eQq_{bb} = eQq(D)[(3\langle\cos^2\theta_b\rangle - 1)/2] \quad (2)$$

acetylene molecular axis upon the a and b inertial axes of the complex. Consequently, $\theta_a = 180° - \theta_2$ and $\theta_b = \theta_2 - 90°$. Since supplementary values of θ_2 relate structures A and B, eqs 1 and 2 do not distinguish between structures A and B.

In order to calculate θ_a and θ_b from eqs 1 and 2, the values of $eQq(D)$ must be measured for C_2HD and C_2D_2 in their ground vibrational states. Although these measurements have not been reported, DeLeon and Muenter argued that the perpendicular component of $eQq(D)$ in the planar complex, Ar–C_2D_2, should accurately approximate the free acetylene monomer $eQq(D)$ value.[31] Recent measurements of Ar–C_2D_2 give $eQq(D) = 208.5$ kHz for the perpendicular component.[32] Still it is not clear if this value should be used for $eQq(D)$ of C_2HD. Marshall and

Structure A

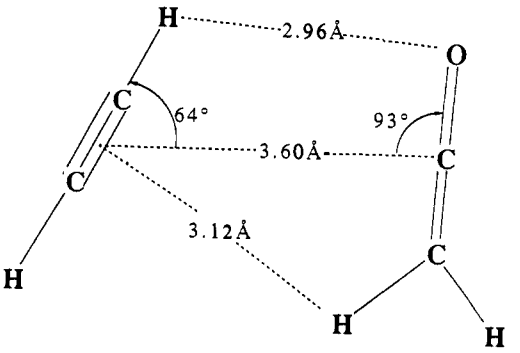

Structure B

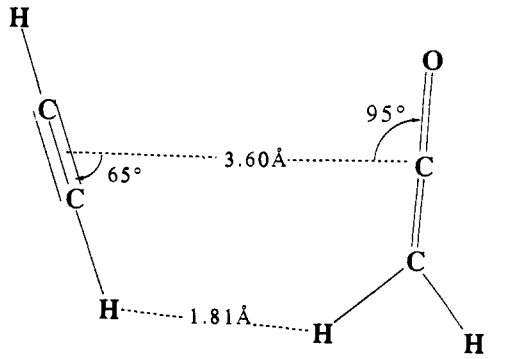

Figure 4. Structures A and B obtained from least-squares fits of the moments of inertia data for four isotopic species to R, θ_1, and θ_2. Structure A is preferred over B due to the short H···H distance of 1.81 Å in B, which destablizes the complex. The dotted lines connecting acetylene and ketene do not indicate directed interactions but simply give distances between specific atoms in the complex.

Klemperer[33] reported a value of $eQq(D) = 221$ kHz for the $\nu_5 = 4$ state of C_2HD, and DeLeon and Muenter[32] find values of 209.2 kHz for $\nu_4 = 1$ and 208.7 kHz for $\nu_5 = 1$ of C_2D_2. Marshall and Klemperer suggest that $eQq(D)$ in the ground state of C_2HD should be taken as 221 kHz, which disagrees slightly with DeLeon and Muenter's value of 208.5 kHz obtained for Ar–C_2D_2.

When eqs 1 and 2 are used with the A_1 state values of eQq_{aa} and eQq_{bb} for CH_2CO–C_2HD listed in Table VI in conjunction with either DeLeon and Muenter's value[32] of $eQq(D) = 208.5$ kHz or Marshall and Klemperer's value[33] of $eQq(D) = 221$ kHz, we find $\theta_a = 62.1$ or 61.7° and $\theta_b = 15.9$ or 19.3°. Similarly, values of $\theta_a = 63.9°$ and $\theta_b = 29.3°$ are obtained from eQq_{aa} and eQq_{bb} listed for CH_2CO–C_2D_2 in Table IV with $eQq(D) = 209$ kHz, the average value of DeLeon and Muenter's measurements of $eQq(D)$ for C_2D_2 in the $\nu_4 = 1$ and $\nu_5 = 1$ excited states. These independent estimates of θ_a and θ_b from the deuterium quadrupole data of CH_2CO–C_2HD and CH_2CO–C_2D_2 compare well with $\theta_a = 64.0°$ $(180° - \theta_2)$ and $\theta_b = 26.0°$ $(\theta - 90°)$ calculated from the value of θ_2 obtained from the r_o moment of inertia fit for structure A in Table IX. The quadrupole coupling constants are considerably better determined for CH_2CO–C_2D_2 than for CH_2CO–C_2HD. It should be noted that differences in θ_a and θ_b calculated from eqs 1 and 2 and from the r_o moment of inertia fit range from less than 1° in θ_a to only about 3° in θ_b. Since θ_a and θ_b are geometrically related to θ_2, these differences provide a qualitative estimate of the zero-point vibrational motion associated with in-plane bending of acetylene in the complex.

D. Internal Motion. Group theoretical methods employed by Coudert *et al.* for H_2O–D_2O[23,34] can be applied to analyze the

(31) DeLeon, R. L.; Muenter, J. S. *J. Chem. Phys.* **1980**, *72*, 6020.
(32) DeLeon, R. L.; Muenter, J. S. *J. Mol. Spectrosc.* **1987**, *126*, 13.
(33) Marshall, M. D.; Klemperer, W. A. *J. Chem. Phys.* **1984**, *81*, 2928.
(34) Coudert, L. H.; Hougen, J. T. *J. Mol. Spectrosc.* **1988**, *130*, 86.

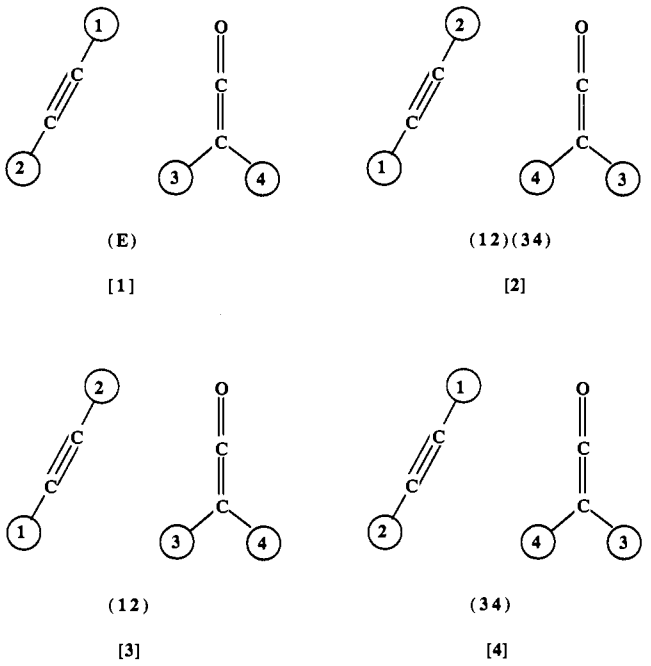

Figure 5. Four equivalent frameworks of CH_2CO–C_2H_2 designated as [1], [2], [3], and [4]. The complex is planar and all atoms are located in the ab plane. The permutation inversion operation to be applied upon the basis function of framework [1] is given in parentheses under that framework.

tunneling motions in CH_2CO–C_2H_2. As illustrated in Figure 5, four equivalent frameworks exist for CH_2CO–C_2H_2 with a planar structure. The [1] → [3] motion interchanges acetylene hydrogens, while the [1] → [4] motion accomplishes the same exchange for the ketene hydrogens. A geared motion represented by [1] → [2] in Figure 5 achieves both acetylene and ketene hydrogen exchange via one path.

Since CH_2CO–C_2H_2 has the same permutation-inversion group as does H_2O–D_2O,[34] each asymmetric rotor energy level is split into four states by tunneling between the four frameworks shown in Figure 5. The four states belong to the symmetry species $A_1^{\pm}$, $A_2^{\pm}$, $B_1^{\pm}$, and $B_2^{\pm}$. Allowed b-type transitions follow the selection rules $A_1^{\pm} \leftrightarrow A_1^{\pm}$, $A_2^{\pm} \leftrightarrow A_2^{\pm}$, $B_1^{\pm} \leftrightarrow B_1^{\pm}$, and $B_2^{\pm} \leftrightarrow B_2^{\pm}$. The two pairs of equivalent hydrogen nuclei have nuclear spin $^1/_2$ and must follow Fermi–Dirac statistics upon exchange by the tunneling motions. Consequently, the nuclear spin statistical weight for the four tunneling states A_1:A_2:B_1:B_2 are 1:3:3:9. In agreement with this theoretical analysis, four components of each b-type transition with relative intensities approximately in the ratios 1:3:3:9 were observed for CH_2CO–C_2H_2 (see Table I and Figure 1). The four components of each b-type transition give rise to the four series designated A_1, A_2, B_1, and B_2 in Table I, and each series fits well to a Watson Hamiltonian (see Table II).

The group theoretical analysis for CD_2CO–C_2H_2 is the same as for CH_2CO–C_2H_2 except that in CD_2CO–C_2H_2 the deuterium nuclei have nuclear spins of 1. Therefore, Bose–Einstein statistics are obeyed for tunneling motions of ketene which exchange the two deuterium nuclei. If the large A–B splitting observed for CH_2CO–C_2H_2 is due to acetylene tunneling and the small A_1–A_2 and B_1–B_2 splittings arise from ketene tunneling, then the four states A_1:A_2:B_1:B_2 in CD_2CO–C_2H_2 will exhibit nuclear spin statistical weights of 2:1:6:3. Four components are observed for each transition as shown in Figure 2 and Table III. While the nuclear spin weights for A_1–A_2 and B_1–B_2 states could not be verified, it is clear from the intensities of a number of transitions that the B state lines are more intense than the A state lines. Comparison of the A_1–A_2 (B_1–B_2) transition splittings in CH_2CO–C_2H_2 (Table I) with the same splittings in CD_2CO–C_2H_2 (Table III) reveals a factor of 5–10 decrease upon deuteration of ketene. This reduction in the A_1–A_2 splitting supports the assignment of the ketene tunneling motion to the smaller splitting in both isotopic forms.

Two structural isomers of CH_2CO–C_2HD are possible since the hydrogen or deuterium of acetylene may be located adjacent to the ketene oxygen (see Figure 3). While the acetylene tunneling is not possible due to the deuterium substitution, ketene hydrogen exchange still leads to two equivalent frameworks for each structural isomer. Hence, each rotational transition will be split into two components by the ketene tunneling motion. These two tunneling states are designated A_1 and A_2 for each structural isomer and must have nuclear spin statistical weights of 1:3, respectively, due to exchange of the ketene hydrogen spin $^1/_2$ nuclei. Both the A_1 and A_2 tunneling states will be further split by the nuclear electric quadrupole moment of the acetylene deuterium nucleus. In principle, four sets of rotational transitions each having nuclear hyperfine structures are possible for CH_2-CO–C_2HD. However, the two structural isomers of CH_2CO–C_2HD are not expected to be isoenergetic due to differences in zero point energies of the two forms. This zero-point isotope effect can be large enough so that only the lowest energy structural isomer is populated in the T = 1 K molecular beam.[4]

The two sets of rotational transitions observed for CH_2CO–C_2HD exhibit similar deuterium hyperfine patterns. Also, the hyperfine free lines for each set are split approximately the same, as found for the A_1–A_2 splitting in CH_2CO–C_2H_2 (compare the A_1–A_2 line frequencies listed in Tables I and V). Finally, one set of lines is approximately a factor of 3 more intense than the other set. These three observations are consistent with an assignment of the two sets of transitions to the A_1 (weak line intensities) and A_2 (strong line intensities) ketene tunneling states of the lowest energy CH_2CO–C_2HD structural isomer. The results discussed in section IIIC indicate that this isomer has the acetylene deuterium located adjacent to the ketene oxygen (structure A in Figure 4).

The CH_2CO–C_2D_2 isotopic species is similar to CH_2CO–C_2H_2 and CD_2CO–C_2H_2 because it also has four equivalent frameworks related by the same permutation inversion operations given in Figure 5. Each rotational transition of CH_2CO–C_2D_2 will be split into four tunneling states designated A_1:A_2:B_1:B_2 with nuclear spin statistical weights of 6:18:3:9, respectively. Even though both CH_2CO–C_2D_2 and CD_2CO–C_2H_2 exchange a pair of spin $^1/_2$ and a pair of spin 1 nuclei through tunneling, significant differences are expected and have been observed in the spectra of the two isotopic species. First, exchange of the deuterium nuclei for acetylene tunneling in CH_2CO–C_2D_2 produces an overall 2:1 spin weight for the A:B states. Then superimposed upon this weight is the 1:3 spin weight for A_1:A_2 and B_1:B_2 due to the ketene hydrogen nuclei exchange. The result is that two intense states, A_2 and B_2, will stand out in the four components of each rotational transition. In addition, the large tunneling splitting due to acetylene in CH_2CO–C_2H_2 will be reduced in CH_2CO–C_2D_2 to approximately the magnitude of the ketene hydrogen splitting, which means that the four components of each line will exhibit similar splittings in CH_2CO–C_2D_2. Furthermore, resolved nuclear hyperfine structure is expected for each tunneling state transition of CH_2CO–C_2D_2 because the nuclear electric quadrupole coupling constants are larger for C_2D_2 than for CD_2CO. If the deuterium nuclei in CH_2CO–C_2D_2 are equivalent due to the acetylene tunneling motion, then the A_1 (A_2) state lines will contain the I = 0 and 2 hyperfine components and the B_1 (B_2) state lines the corresponding I = 1 components. The deuterium hyperfine analysis given in Tables VII and VIII for the two most intense tunneling states, A_2 and B_2, provides strong support for acetylene tunneling in CH_2CO–C_2D_2. Unfortunately, the less intense A_1 and B_1 states could not be fully assigned (see the discussion in section IIIA) so that the evidence for ketene tunneling in CH_2CO–C_2D_2 is less definitive. However,

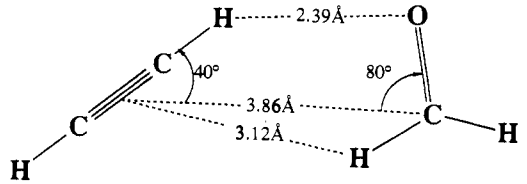

Figure 6. Microwave structure of CH_2O–C_2H_2 reported in ref 30.

the presence of additional lines observed at approximately the expected frequencies for several of the more intense rotational transitions suggests ketene tunneling is taking place in CH_2CO–C_2D_2.

The spectroscopic data discussed above for the four isotopic species are consistent with internal motions in the complex which exchange the hydrogen nuclei of both ketene and acetylene. They do not distinguish between the geared [1] → [2] versus independent [1] → [3] and [1] → [4] tunneling paths in Figure 5. If the tunneling motion is simply a C_2 rotation about the molecular axis of ketene (I_a = 1.79 u Å^2) and the b axis of acetylene (I_b = 14.3273 u Å^2), i.e. independent [1] → [3] and [1] → [4] paths, then the smaller reduced mass of the ketene motion should give rise to larger spectral splittings. Since this is contrary to the observations in ketene–acetylene complex, it follows that the barrier to acetylene hydrogen exchange is lower than the corresponding barrier for ketene hydrogen exchange.

IV. Discussion

A. Structure and Internal Motion. The planar geometry of CH_2CO–C_2H_2 qualitatively resembles the planar structure of CH_2O–C_2H_2 shown in Figure 6. Howard and Legon interpreted the weak intermolecular binding of CH_2O–C_2H_2 in terms of two nonlinear hydrogen interactions.[30] One is between the formaldehyde oxygen and acetylenic hydrogen, r(O···H) = 2.39 Å, and the other is between a formaldehyde hydrogen and the acetylene π bond, r(H···π center) = 3.12 Å. Since the ketene oxygen acetylene hydrogen distance is quite long, r(O···H) = 2.96 Å, CH_2CO–C_2H_2 is probably not a hydrogen bonded complex. Estimates of the van der Waals bond force constant from the quartic centrifugal distortion constant, Δ_J, indicate that ketene does not bind as strongly to acetylene as does formaldehyde. Using the equation developed by Millen for a planar complex,[35] a force constant of 2.36(1) N/m is obtained for CH_2CO–C_2H_2 which, compares to the larger force constant of 2.842(2) N/m calculated for CH_2O–C_2H_2. Electrostatic modeling using distributed multipole analysis for CH_2CO–C_2H_2 shows that quadrupole–quadrupole interactions between ketene and acetylene make the largest contribution to the binding energy.[36] This result suggests that a weak multicentered interaction accounts for the binding in CH_2CO–C_2H_2 rather than the directed O···H and π···H interactions described for CH_2O–C_2H_2.[30]

There are also distinct differences in the internal motions of the two complexes. Splittings of spectral transitions, observed relative intensities consistent with nuclear spin statistical weights, and deuterium hyperfine effects provide strong evidence that both the ketene and acetylene hydrogen nuclei in CH_2CO–C_2H_2 are exchanged by tunneling motions. In CH_2O–C_2H_2 the spectral transitions are split by internal motions involving the formaldehyde subunit.[30] The two observed states are of unequal intensity, and the less intense state was assigned to a low-lying excited vibration involving an out-of-plane large amplitude torsion about the C=O bond of formaldehyde. Deuterium substitution in acetylene does not affect the excited state significantly, and there is no additional splitting of the spectral transitions. Consequently, there is no evidence from the rotational spectroscopic data of internal motions involving acetylene. The acetylene tunneling observed in CH_2CO–C_2H_2 may arise from a lower barrier which is due to a weaker interaction between ketene and acetylene than what exists between formaldehyde and acetylene.

The difference noted above in the ketene and formaldehyde internal motions of the two complexes is difficult to establish from the experimental data. Tunneling motions that cause spectral splittings of rotational transitions give rise to nuclear spin statistical weights which differ for the tunneling states. If the nuclei which are exchanged by the tunneling motion have resolvable electric quadrupole structure, then the even or odd nuclear spin states are absent from a rotational transition of a given tunneling state. Excited states arising from a large amplitude torsional motion such as is suggested for the formaldehyde–acetylene complex will not exhibit the above effect from nuclear spin statistical weights or the nuclear hyperfine effects for CD_2O–C_2H_2, which has a deuterium electric quadrupole moment. Since neither CD_2CO–C_2H_2 nor CD_2O–C_2H_2 have resolvable nuclear hyperfine transitions, it is not possible to use the deuterium electric quadrupole structure to distinguish between torsional motion or tunneling of ketene or formaldehyde. However, intensity measurements for CH_2CO–C_2H_2 do show the 1:3 nuclear spin statistical weights expected for exchange of the ketene hydrogen nuclei. It is important to note that the exchange motion can give rise to two tunneling states in CH_2CO–C_2H_2 even though the ketene hydrogens are nonequivalent in the planar configuration (see Figure 5). This is also true for the nonequivalent acetylene hydrogens in CH_2CO–C_2H_2, and in fact, the observed nuclear spin weights provide evidence that both the ketene and acetylene hydrogen nuclei are tunneling. In CH_2O–C_2H_2 the splitting of the spectral transitions is so small that the pairs of lines from the two vibrational states fall within the band width of the microwave cavity, and as a result, the intensities are critically dependent on the cavity resonance positioning relative to the microwave pump frequency. Hence, it is more difficult to make reliable intensity measurements, which means that it is not easy to distinguish between tunneling states and an excited vibrational state arising from torsion of the hydrogen atoms about the C=O axis in formaldehyde.

B. Ketene–Acetylene Complex and (2 + 2) Cycloaddition Reactions. As discussed in the Introduction, there is a strong resemblance of the structures of O_3–C_2H_4 and O_3–C_2H_2 van der Waals complexes with the envelope conformations of the transition states predicted by orbital symmetry analyses for 1,3-dipolar cycloaddition reactions.[4,5] However, theoretical results show negligible π overlap between the carbons of C_2H_4[4] (as well as C_2H_2[5]) and the terminal oxygens of O_3 at the measured C···O van der Waals separations of >3.0 Å. These calculations indicate that the stability and geometry of the two complexes are determined by long-range electrical interactions. Even though π overlap appears not to be significant, it is interesting that the HOMO–LUMO π interactions mimic the longer-range electrical interactions which are responsible for the binding of O_3 to C_2H_2 and C_2H_4.

In the cycloadditions of ketene to ethylene or acetylene, the orbital interactions are complicated by the mutually orthogonal C=C and C=O orbitals of ketene. The ketene–ethylene cycloaddition is a classical example of a concerted ($2\pi_s + 2\pi_a$) reaction. According to Woodward and Hoffmann, the C=C of ketene acts as the antarafacial $2\pi_a$ component which forms two bonds with the supra $2\pi_s$ C=C system of ethylene.[12] They also proposed interactions between the HOMO of ethylene and the low-lying π^* C=O orbital of ketene. The ($2\pi_s + 2\pi_a$) approach of ethylene to ketene leads to a perpendicular crossed orientation of the molecular planes in the transition state (see I in the Introduction). A number of quite different orbital interactions have been considered in recent theoretical studies of the ketene–ethylene cycloaddition.[13-18] Although some of these studies use parallel approaches of the C=C=O and C=C axes of ketene

(35) Millen, D. J. *Can. J. Chem.* **1985**, *63*, 1477.
(36) Fowler, P. W.; Gillies, C. W.; Gillies, J. Z.; Kisiel, Z.; Lovas, F. J.; Suenram, R. D. *J. Am. Chem. Soc.*, to be submitted.

and ethylene,[15,16] the transition states have nonplanar heavy atom geometries in which the molecular planes of ketene and ethylene are crossed with C–C bond formation advanced at the carbonyl carbon of ketene.[13-18] A recent study of the ketene-ethylene van der Waals adduct finds that the molecular planes are crossed as predicted by $(2\pi_s + 2\pi_a)$ orbital interactions.[36,37]

The *ab initio* investigation of ketene plus acetylene interprets the reaction in terms of a $(2\pi_s + 2\pi_a)$ cycloaddition which gives the crossed configuration shown as III below.[18] An optimized transition-state geometry was obtained by gradient techniques employing a minimal STO-3G basis set. This calculation finds the molecular axes of ketene and acetylene to be slightly crossed with a dihedral angle of $\angle C_4C_3C_2C_1 = -24.1°$. The C–C bond formation is more advanced at the ketene carbonyl carbon, $r(C_2C_1) = 1.905$ Å, than at the methylene carbon, $r(C_3C_4) = 2.197$ Å. Since the equilibrium geometry of the ketene–acetylene complex

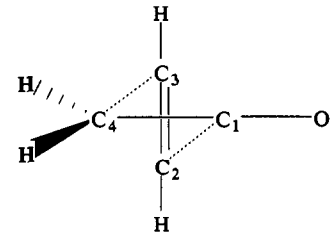

III

is planar, this structure differs significantly from the one described above for a $(2\pi_a + 2\pi_s)$ orbital interaction. Higher level *ab initio* calculations are needed to characterize the van der Waals and reaction potential surfaces of ketene plus acetylene.

Acknowledgment. This research was partially supported by a grant from the Research Corp. to C.W.G.

(37) Lovas, F. J.; Suenram, R. D.; Gillies, C. W.; Gillies, J. Z. *46th Symp. Mol. Spectrosc.* **1991**, TE8.